Selective inhibitors of the TrkC.T1 receptor reduce retinal inflammation and delay neuronal death in a model of retinitis pigmentosa

Fouad Brahimi [ID][a], Hassan Nassour [ID][a,b], Alba Galan[a], Revathy Guruswamy [ID][b], Christina Ortiz[a], Ali Nejatie [ID][a,b], Hinyu Nedev[a], Jean-Francois Trempe [ID][b,c,d,e] and H. Uri Saragovi [ID][a,b,e,f,*]

[a]Lady Davis Institute—Jewish General Hospital, McGill University, Center for Translational Research, Montreal, QC, Canada H3T 1E2
[b]Pharmacology and Therapeutics, McGill University, Montreal, QC, Canada H3G 1Y6
[c]Centre de Recherche en Biologie Structurale, McGill University, Montreal, QC, Canada H3G 1Y6
[d]Structural Genomics Consortium, McGill University, Montreal, QC, Canada H3G 1Y6
[e]Brain Repair and Integrative Neuroscience (BRaIN), McGill University, Montreal, QC, Canada H3G 1Y6
[f]Ophthalmology and Vision Science, McGill University, Montreal, QC, Canada H3T 1E2
*To whom correspondence should be addressed: Email: uri.saragovi@mcgill.ca
Edited By Andrey Abramov

Abstract

The heterogeneity of receptor isoforms can cause an apparent paradox where each isoform can promote different or even opposite biological pathways. One example is the neurotrophin receptor TrkC. The *trkC* mRNA translates a full-length receptor tyrosine kinase (TrkC-FL) whose activation by the growth factor NT3 promotes neuronal survival. In some diseases, the *trkC* mRNA is spliced to a kinase-truncated isoform (TrkC.T1) whose activation by NT3 up-regulates tumor necrosis factor alpha (TNF-α) causing neurotoxicity. Since TrkC.T1 expression is significantly increased at the onset of neurodegeneration, we hypothesized that in disease TrkC.T1-mediated toxicity prevails over TrkC-FL-mediated survival. To study this, we developed small molecules that selectively antagonize NT3-driven TrkC.T1 neurotoxicity without compromising TrkC-FL survival. In a genetic mouse model of retinitis pigmentosa, therapeutic administration of TrkC.T1 antagonists prevents elevation of TNF-α and reduces photoreceptor neuronal death. This work demonstrates the importance of accounting for functional and structural heterogeneity in receptor–ligand interactions, illustrates chemical biology strategies to develop isoform-selective agents, validates TrkC.T1 as a druggable target, and expands the therapeutic concept of reducing neurotoxicity as a strategy to achieve neuroprotection.

Keywords: TrkC receptor isoform, neurotoxicity, neuroprotection, chemical biology, photoreceptor

Significance Statement

TrkC-FL is expressed in neurons, and the ligands NT3 or protein tyrosine phosphatase-sigma (PTPs) directly activate neuronal survival signals. The TrkC.T1 isoform is up-regulated in glia during disease. Paradoxically, TrkC.T1•NT3 induces tumor necrosis factor alpha (TNF-α) which causes paracrine neuronal death, whereas TrkC.T1•PTPs can induce synaptic stability but does not induce TNF-α or neuronal death. To target TrkC.T1-mediated neurotoxicity, we used chemical biology to develop small molecules that selectively antagonize TrkC.T1•NT3 but do not inhibit TrkC-FL•NT3 and do not affect the binding of PTPs to either isoform. Agents reduce TNF-α and neuronal death in a genetic mouse model of retinitis pigmentosa where TrkC.T1 activity is etiological to neurodegeneration. The work validates TrkC.T1 as a druggable target, and "antineurotoxicity" as a means to achieve neuroprotection. The concept may be applicable to receptor–ligand families with isoforms where different extracellular conformations can be targeted.

Introduction

TrkC receptors are expressed in neurons (1–3), in vascular endothelium (4, 5), and in glia and microglia (6, 7). The *trkC* mRNA can translate a full-length protein (TrkC-FL) which has an intracellular tyrosine kinase catalytic domain and is the major TrkC isoform in normal healthy adult tissues. The *trkC* mRNA is alternatively spliced in exons, resulting in the deletion of the kinase domain and the gain of a short unique intracellular sequence. The resulting truncated isoform is called TrkC.T1 (8, 9).

Both TrkC-FL and TrkC.T1 share the same ligand-binding ecto-domain primary sequence (8–11). Both isoforms bind the same activating ligands: the soluble growth factor neurotrophin-3 (NT3), and the membrane-bound protein tyrosine phosphatase-sigma (PTPs). The affinity of NT3 for each isoform and the affinity of PTPs for each isoform are indistinguishable (12, 13).

Activation of neuronal TrkC-FL by NT3 or by PTPs mediates "positive" signals through the tyrosine kinase catalytic activity that phosphorylates downstream signals in neurons (pPI3K, pErk1,2, pAkt), resulting in neuronal survival. In neurons, in addition to survival, NT3•TrkC-FL also promotes neuronal growth/differentiation (11, 14), and PTPs•TrkC-FL also promotes synaptic stabilization (13). In contrast, NT3 activation of TrkC.T1 expressed in glia stimulates glial tumor necrosis factor alpha (TNF-α) production to toxic levels, which causes neuronal death (10, 15). However, PTPs activation of TrkC.T1 expressed in glia does not stimulate TNF-α production (11). Together, these data indicate a signaling bias by NT3 and PTPs as agonists of each isoform, and the ability of each receptor isoform to induce different and sometimes opposite biological outcomes. This is in part due to the intrinsic signals of each isoform, to the biased activation of signaling pathways by each ligand, and to the cell types in which each isoform is expressed (14).

Early at the onset of certain neurodegenerative diseases (e.g. experimental models of glaucoma, amyotropic lateral sclerosis (ALS), and retinitis pigmentosa [RP]; and human sporadic ALS) TrkC.T1 mRNA and protein, as well as NT3, are significantly up-regulated in glia and microglia (6, 10, 11, 15, 16). This results in production of high levels of TNF-α which causes neurotoxicity. Reducing TrkC.T1 expression that up-regulates in vivo during disease prevents TNF-α up-regulation and slows down disease progression (6, 10, 11, 15, 16), demonstrating an etiological role for TrkC.T1. In this context, we proposed a strategy to differentially target TrkC-FL and TrkC.T1 therapeutically (14).

We previously reported selective agonists of TrkC-FL (that do not activate TrkC.T1). These agents promote survival signals in TrkC-FL-expressing neurons, without promoting TNF-α toxicity by TrkC.T1-expressing glia (10). Selective TrkC-FL agonists are highly effective therapeutically in vivo in a mouse model of ALS, protecting TrkC-FL-expressing motor neurons even though TrkC.T1 is up-regulated in spinal cord glia (11).

The focus of the present work is a second and complementary strategy, to develop antagonists of TrkC.T1 (that do not antagonize TrkC-FL) to address the remaining problem of TrkC.T1-mediated toxicity induced by NT3. The optimal antagonists should inhibit NT3•TrkC.T1, but not inhibit PTPs•TrkC.T1 because PTPs does not induce toxicity.

Using chemical biology strategies, we developed biased antagonists of NT3•TrkC.T1-driven neurotoxicity, that do not impact on PTPs ligand binding or activity. Antagonism is TrkC.T1 isoform specific, with no effect on TrkC-FL activation by any ligand. Computational modeling and docking suggest that the small molecules bind at the interface of the immunoglobulin-like D4–D5 subdomains of TrkC.T1, adjacent to the D5 domain, where NT3 binds but distant from the leucine-rich motifs-like D1–D2 subdomains where PTPs binds. Two structurally related antagonists are therapeutic in a mouse model of RP where TrkC.T1 and NT3 are up-regulated in Müller glia (15, 16).

This work supports the concept that accounting for the functional and structural heterogeneity of receptor–ligand interactions can improve targeted therapies, including novel neuroprotection strategies to "enhance survival" or to "reduce neurotoxicity," and validates TrkC.T1 as a druggable therapeutic target.
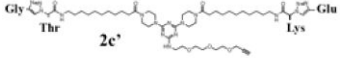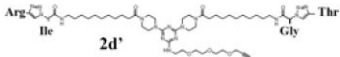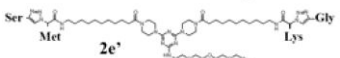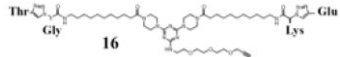
Results
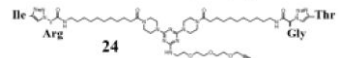
TrkC.T1-based screening of previously reported TrkC-FL ligands

We have reported agents displaying amino acid side chains R^1R^2-R^3R^4 (17) in a β-turn conformation mimicking the $i+1$ and $i+2$ residues of the β-turns of neurotrophins (17–20). Agents **2c'**, **2d'**, and **2e'** (respectively, GT-EK, RI-TG, and SM-GK amino acid side chains) mimic a β-turn conformation and pharmacophore of neurotrophins (17–20). **2c'**, **2d'**, and **2e'** bind to TrkC-FL and functionally modulate TrkC-FL•NT3 activity (20–23). The structures are shown in Table 1.

However, our original work evaluated the agents only with regards to the TrkC-FL isoform and was not evaluated on the TrkC.T1 isoform. This omission arose because at that time, a differential binding of agents to the isoforms was unexpected. As, we demonstrated, it is possible to generate TrkC-FL isoform-selective agents (11), we searched for that TrkC.T1 isoform-selective agents.

2c', **2d'**, and **2e'** were re-screened on TrkC.T1 isoforms. For direct receptor-binding assays, the agents were tagged with biotin (Fig. 1A). In quantitative flow cytometry–binding assays using isogeneic transfected cells, biotinylated **2c'**, **2d'**, and **2e'** b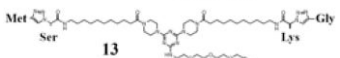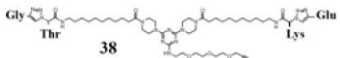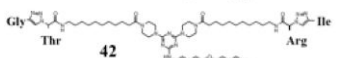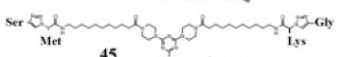ind to cells expressing stably transfected TrkC-FL (confirming earlier reports; Fig. 1B), and they also bind to cells expressing stably transfected TrkC.T1 (Fig. 1C). Quantification of three independent assays standarizing vs. control parental nontransfected cells (not expressing any TrkC) showed that binding is significantly higher to TrkC-FL or to TrkC.T1-expressing cells (Fig. 1D).

Table 1. Reported TrkC-FL antagonists and analogs.

	R^1R^2-R^3R^4	R^4R^3-R^2R^1	R^2R^1-R^4R^3
Class A	(GT-EK) **2c'**	(KE-GT) **16**	(TG-EK) **38**
Class B	(RI-TG) **2d'**	(GT-RI) **24**	(TG-IR) **42**
Class C	(SM-GK) **2e'**	(KG-SM) **13**	(MS-GK) **45**

Published agents **2c'** and **2e'** antagonize TrkC-FL, whereas **2d'** antagonizes both TrkC-FL and TrkC.T1. Analogs **16** and **42** only antagonize TrkC.T1. Antagonism is biased to NT3, as the agents do not impact PTPs binding or function. Chemical structures are shown.
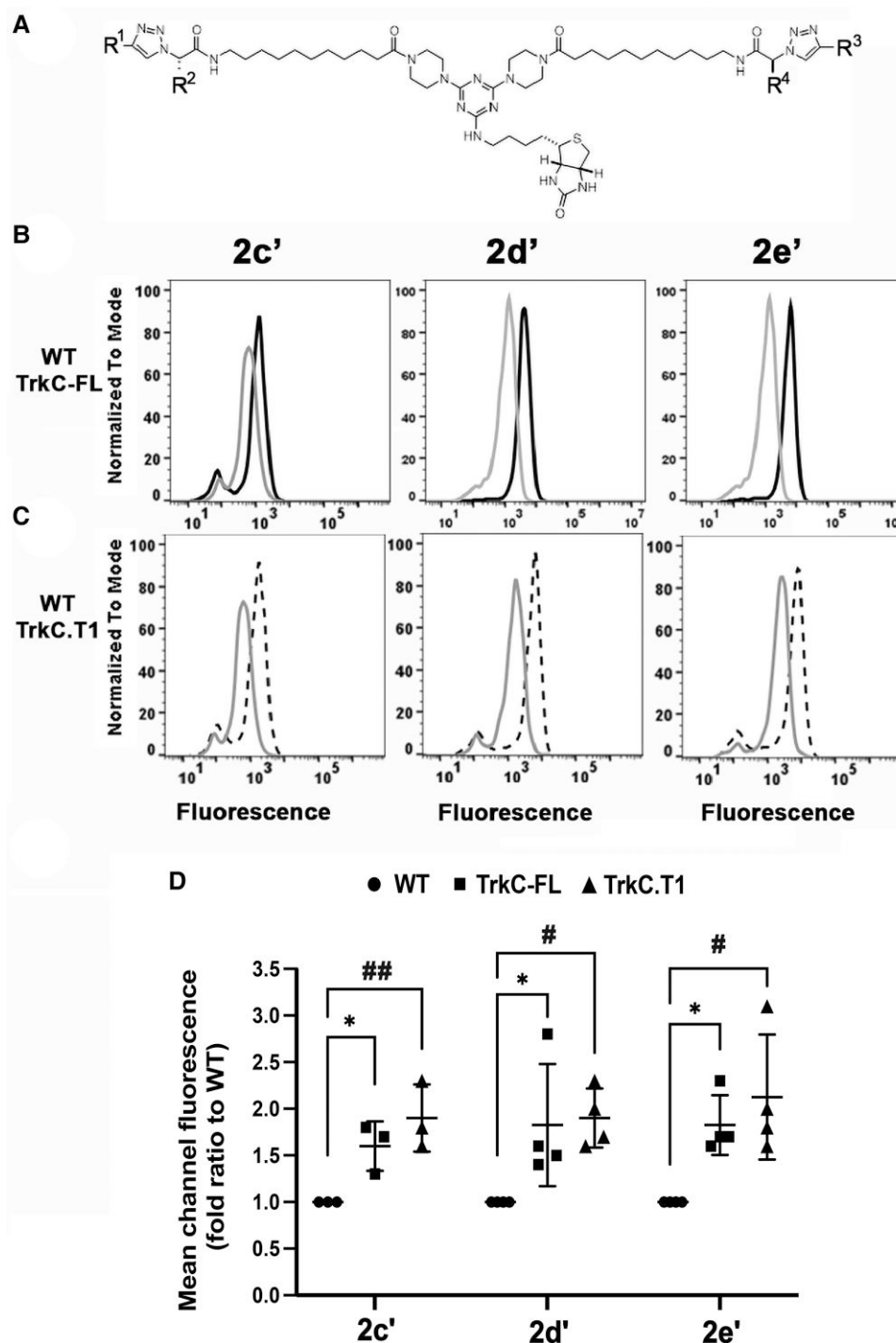
Fig. 1. 2c', 2d', and 2e' bind to TrkC-FL and to TrkC.T1. A) Triazole backbone displaying side chains R1, R2, R3, and R4 (amino acids are listed in Table 1). The optional biotin tag is added to facilitate direct binding studies by flow cytometry. B and C) Histograms of flow cytometry–binding assays. The indicated biotinylated agents (10 μM) were incubated at 4 °C with cells expressing either TrkC-FL or TrkC.T1, or control WT cells not expressing any TrkC, followed by avidin-FITC. Cells were analyzed live by flow cytometry. The compounds **2c', 2d', and 2e'** are reported as TrkC-FL binding but they were not previously tested on TrkC.T1-expressing cells. D) Quantification of flow cytometry–binding assays ($n = 3$ independent experiments averaged $\pm$ SD), with each independent assay standardized to the mean fluorescence of background WT cells set as 1. Data reported as fold-increase over background. One-way ANOVA with significance $\alpha < 0.05$ followed by Bonferroni's correction. Symbols indicate statistical differences in binding compared with WT cells (* or # $P < 0.05$, ## $P < 0.01$). There are no statistical differences in binding between TrkC-FL and TrkC.T1.

Next, we studied the functional impact of these agents on the signals promoted by NT3. Agent **2d'** significantly inhibits TrkC.T1•NT3-promoted up-regulation of TNF-α mRNA, but **2c'** and **2e'** do not inhibit significantly (Fig. 2A, **2e'** is $P = 0.09$, Table 2). The effective antagonistic concentrations of **2d'** are nontoxic (Fig. S1A); hence, inhibition is not due to cell death.

All the agents are antagonists of TrkC-FL•NT3, and lower the cell survival promoted by NT3 in serum-deprived cultures (Fig. 2B). Hence, all agents bind to both isoforms and antagonize NT3•TrkC-FL, but only **2d'** is a functional antagonist of NT3•TrkC.T1. Note that these agents are TrkC selective, because in counter assays, they did not have any effect on the survival

Fig. 2. **2d'** is an antagonist of NT3 activation for both TrkC isoforms. A) In TrkC.T1-expressing cells, **2d'** inhibits NT3-promoted TNF-α expression. Data are quantitative real-time PCR aft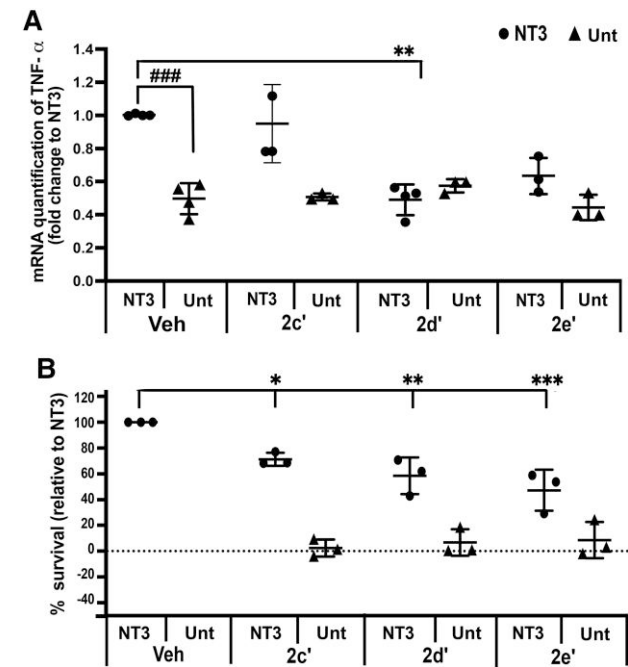er 6 h of the indicated treatment [±NT3 (4 nM) ± 10 μM of test agents], standardized to the control treatment (vehicle [Veh] + NT3) set as 100%. Data are the mean ± SD of at least three independent experiments, each in triplicate. One-way ANOVA with significance α < 0.05 followed by Bonferroni's correction for multicomparisons showed significant differences. Veh untreated is significantly lower than Veh + NT3 (###$P < 0.001$). Agent **2d'** + NT3 is significantly lower compared with Veh + NT3 (**$P < 0.01$). There are no differences between Veh untreated and **2d'** + NT3, meaning that all the increased TNF-α expression is inhibited. There are no differences between Veh untreated and Veh ± test agents, meaning that in the absence of NT3 the agents do not promote TNF-α expression (i.e. there is no partial agonistic activity), and that agents do not induce cell death (i.e. no cellular toxicity). Other statistical differences are omitted in the graph for clarity. B) In TrkC-FL-expressing cells, all test agents (**2c'**, **2d'**, and **2e'**) antagonize cell survival promoted by NT3. Cells cultured in serum-free conditions (to induce death) were treated for 48 h ± agents (10 μM) ± optimal concentrations of NT3 (2 nM). Data are standardized to Veh + NT3 treatment set as 100% cell survival. Shown are the mean + SD of at least three independent experiments, each in triplicate wells. One-way ANOVA with significance α < 0.05 followed by Bonferroni's correction for multicomparisons show a significant reduction in cell survival when comparing Veh + NT3 vs. test agents + NT3 (*$P < 0.05$, **$P < 0.01$, ***$P < 0.001$). In the absence of NT3, the agents did not impact cell death, indicating no partial agonistic activity and no toxicity.

Table 2. Summary of functional assays.

Receptor antagonized	TrkC.T1	TrkC-FL	
Ligand antagonized	NT3	NT3	PTPs
Analogs of nonselective antagonists			
Class A			
2c'	−	+	−
16	+	−	−
38	−	−	−
Class B			
2d'	+	+	−
24	−	−	−
42	+	−	−
Class C			
2e'	±	+	−
13	−	−	−
45	−	−	−
1Aa analogs			
Cyclic-14-KI (CP14)	+	−	−
Cyclic-15-KI (CP15)	+	−	−
Cyclic-15-OI	+	−	−
Linear-14-KI	−	−	−
Linear-15-KI	−	−	−

−: no effect detected.
+ on TrkC.T1 column: antagonist for TrkC.T1•NT3 (reduced NT3-induced TNF-α up-regulation).
+ on TrkC-FL column: antagonist for TrkC-FL (reduced NT3-induced activation of pAkt, pErk1,2; reduced cell survival induced by NT3).
±: borderline inhibition ($P = 0.09$) was not evaluated further due to lack of isoform specificity.

(reported data) and of NT3•TrkC.T1 (new data). Interestingly, **2d'** does not antagonize PTPs, in terms of PTPs•TrkC-FL binding or function and in terms of PTPs•TrkC.T1 binding (new data). Therefore, functionally **2d'** is a biased antagonist of NT3.

Analogs of 2d' are selective TrkC.T1 antagonists

We screened analogs of the **2d'** pharmacophore (RI-TG) for NT3•TrkC.T1 selectivity. Analogs were coupled on a backbone in the "forward" and "reverse" orientation (e.g. R^1R^2-R^3R^4 or R^2R^1-R^4R^3) (17). The structures of the compounds are shown in Table 1. Class A analogs related to **2c'** (GT-EK) are 16 (KE-GT) and 38 (TG-EK). Class B analogs related to **2d'** (RI-TG) are 24 (GT-RI) and 42 (TG-IR). Class C analogs related to **2e'** (SM-GK) are 13 (KG-SM) and 45 (MS-GK). These agents were screened for antagonism of TrkC-FL and/or TrkC.T1 (Fig. 4), at concentrations that are nontoxic to cells (Fig. S1B).

Using functional assays, 16 and 42 significantly inhibit NT3•TrkC.T1 function, blocking up-regulation of TNF-α mRNA, but 24, 38, 13, and 45 do not (Fig. 4A). In the absence of NT3, none of the agents impacts the baseline TNF-α expression, further supporting the notion that the agents are not partial agonists and are not toxic. Using quantitative flow cytometry–based competition assays, 16 and 42 do not inhibit PTPs-Fc binding to TrkC.T1 or TrkC-FL (Fig. 4B), indicating that these agents are biased to inhibiting NT3 and not PTPs.

Regarding isoform selectivity, functional counter assays demonstrated no impact on NT3•TrkC-FL-induced biochemical signals (Fig. 4C, quantified in Fig. 4D) or PTPs•TrkC-FL–induced biochemical signals (Fig. 4E, quantified in Fig. 4F). Moreover, in cell survival bioassays using cells induced to die by culture in serum-free conditions, the agents do not antagonize NT3•TrkC-FL-induced survival (Fig. S2A) or PTPs•TrkC-FL-induced survival (Fig. S2B). These biological assays are consistent with the biochemical data, and further confirm that the effective concentrations that inhibit NT3•TrkC.T1 are nontoxic to cells (Fig. S1A and B).

promoted by growth factor and receptor family members NGF•TrkA or BDNF•TrkB (17).

Next, we evaluated whether **2c'**, **2d'**, and **2e'** antagonize PTPs. PTPs binds to TrkC at the LRR-like D1–D2 subdomains, an epitope different than NT3, which binds to the IgG-like D5 subdomain. PTPs•TrkC binding was studied by quantitative flow cytometry using the ectodomain of PTPs tagged with the Fc domain of immunoglobulin (PTPs-Fc). The agents **2c'**, **2d'**, and **2e'** do not block PTPs-Fc binding to either TrkC.T1 or TrkC-FL (Fig. 3A) and do not inhibit PTPs•TrkC-FL promotion of cell survival in serum-free cultures (Fig. 3B). Note that the biological action of PTPs•TrkC.T1 cannot be evaluated, because PTPs does not promote up-regulation of TNF-α (11).

In sum, **2d'** binds to TrkC-FL (reported data) and to TrkC.T1 (new data), and functionally **2d'** is an antagonist of NT3•TrkC-FL
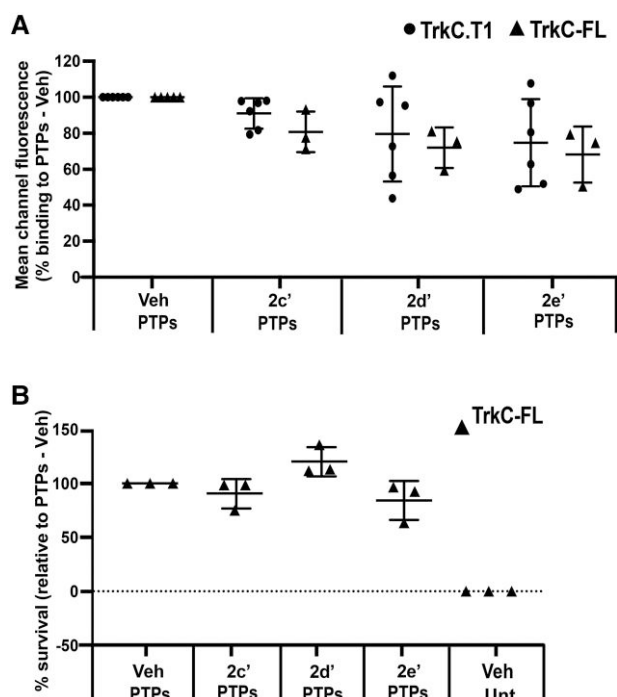
Fig. 3. Compound **2d'** does not impact PTPs•TrkC.T1 binding or PTPs•TrkC-FL binding or functional signals; and is a biased antagonist of NT3•TrkC. A) The agents (10 μM) do not inhibit the binding of PTPs-Fc (40 nM) to cells expressing TrkC-FL or TrkC.T1. Quantitative PTPs-binding competition assays by flow cytometry. The MFC values for PTPs-Fc + vehicle (Veh) control is standardized to 100% binding for each cell type. Shown are the mean ± SD of three independent experiments each acquiring 10,000 cells. Agents **2c'**, **2d'**, and **2e'** do not inhibit PTPs-Fc binding to either TrkC isoform. B) In cells cultured in serum-free conditions to induce cell death, the agents (10 μM) do not inhibit PTPs-promoted (40 nM) TrkC-FL-mediated cell survival. Data were standardized to PTPs-Fc + Veh control set as 100% survival. Shown are the mean + SD of three independent experiments, each independent assay in triplicate wells. Agents **2c'**, **2d'**, and **2e'** do not antagonize PTPs-promoted survival via TrkC-FL and are therefore biased to antagonism of NT3•TrkC.

In sum, these data show that **16** (KE-GT) and **42** (TG-IR) selectively antagonize NT3•TrkC.T1, but do not impact on NT3•TrkC-FL. Antagonism is biased to NT3 because the agents do not affect PTPs binding to either isoform or PTPs•TrkC-FL function. Moreover, the agents do not have intrinsic partial agonistic activity at TrkC.T1 (e.g. in the absence of NT3), and TrkC.T1 functional inhibition is not due to toxic effects. These are desirable pharmacological properties for a selective NT3•TrkC.T1 antagonist.

Converting a nonselective TrkC ligand into a selective TrkC.T1 antagonist

As a second chemical biology strategy for developing antagonists, we investigated analogs of a reported small molecule **1Aa** (20) which binds both TrkC-FL and TrkC.T1 and is an agonist of both isoforms (11). We aimed to develop an analog of **1Aa** that is selective for TrkC.T1 and acts as an antagonist.

1Aa displays IK amino acid side chains in a β-turn conformation (20). We designed cyclic analogs displaying IK on a constrained ring of different sizes. The linear counterparts (not in a β-turn conformation) were synthesized as controls (Fig. 5A). Two analogs, **cyclic-14-KI (CP14)** and **cyclic-15-KI (CP15)** (respectively, on a 14-member ring or a 15-member ring) are functional antagonists of NT3•TrkC.T1 and significantly block up-regulation of

TNF-α (Fig. 5B). In NT3•TrkC-FL, counter assays for selectivity **CP14** and **CP15** do not affect survival-promoting activity (Fig. 5C). These agents are likely biased to NT3 antagonism because in quantitative flow cytometry competition assays, they do not inhibit PTPs-Fc binding to TrkC-FL or to TrkC.T1 (Fig. 5D) and they do not impact on PTPs•TrkC-FL survival-promoting activity (Fig. 5E). Moreover, in receptor selectivity counter assays, the cyclic analogs do not have any effect on receptor family members TrkA or TrkB that are activated by their respective ligands NGF or BDNF (Fig. S3A and B). The relevance of the β-turn structure in the agents is highlighted by the fact that their linear counterparts (not cyclized) have no impact on any assay (NT3•TrkC-FL function; Fig. 5C), PTPs•TrkC-FL binding (Fig. 5D), or NT3•TrkC.T1 function (Fig. S3C).

Together, the data indicate that **CP14** and **CP15** are selective NT3•TrkC.T1 antagonists, do not affect NT3•TrkC-FL, and do not affect PTPs binding to either of the TrkC receptor isoforms. These results support the concept that it is possible to develop an isoform-selective small molecule antagonist starting with a nonselective TrkC ligand **1Aa**.

CP14 selectively reduces the affinity of NT3 for TrkC.T1

We tested the binding of biotin-labeled NT3 (NT3-bio) to TrkC-FL or to TrkC.T1 in flow cytometry–based assays. NT3-bio binds to the receptors in a dose-dependent manner reaching maximal binding (B_{max}) at ~5–10 nM (0–80 nM concentration range was tested). Representative data are shown for NT3-bio binding (0, 0.625, 1.25, and 5 nM) on TrkC-FL and TrkC.T. Binding is specific and competed by nonbiotinylated NT3 ("cold"), where pre-exposure of cells to cold NT3 (10 nM) blocks >80% of the binding of NT3-bio (5 nM) (Fig. S4A and B).

Using this binding assay, we evaluated the impact of compound **16** or **CP14** on the binding of NT3-bio on the TrkC isoforms (Table 3). A range of different agent:ligand stoichiometries was tested (0, 1, 5, and 15 μM agents each vs. 0–80 nM NT3-bio). Representative binding data are shown for 5 μM **CP14** vs. 5 nM NT3-bio (Fig. S4C and D). From the binding constants at different stoichiometries, we determined the K_d of NT3 ± antagonist (Table 3).

NT3 binds to TrkC.T1 with a K_d 1.8 nM, and **CP14** reduces the affinity in a dose-dependent manner to K_d 11.5 nM (a 6.4-fold loss in affinity). Compound **16** causes a less significant 1.7-fold reduction in affinity for TrkC.T1. In contrast, and as internal specificity control, the agents do not affect the affinity of NT3 for TrkC-FL (Table 3). The data suggest that the NT3 inhibitory mechanism of **CP14** is noncompetitive and allosteric, and specific for TrkC.T1. Moreover, it is noteworthy to restate that **CP14** is also biased to inhibiting NT3 and does not impact the binding of PTPs-Fc to either receptor isoform (see above Figs. 4B and E, 5C, D, and E).

Molecular docking of CP14 suggests noncompetitive and allosteric mechanism

To gain insight into the mode of action of CP14, we performed molecular docking using the 3D structure of TrkC as a target. While there are crystal structures of isolated subdomains of human TrkC, including the NT3-binding IgG-C2 (D5) subdomain (PDB 1WWC) (24), there are no experimental 3D structures of the entire human TrkC extracellular ligand-binding domains (ECD), nor for its T1 splice isoform, nor structures bound to the ligands NT3 or PTPRS. To model these structures of TrkC, we thus used
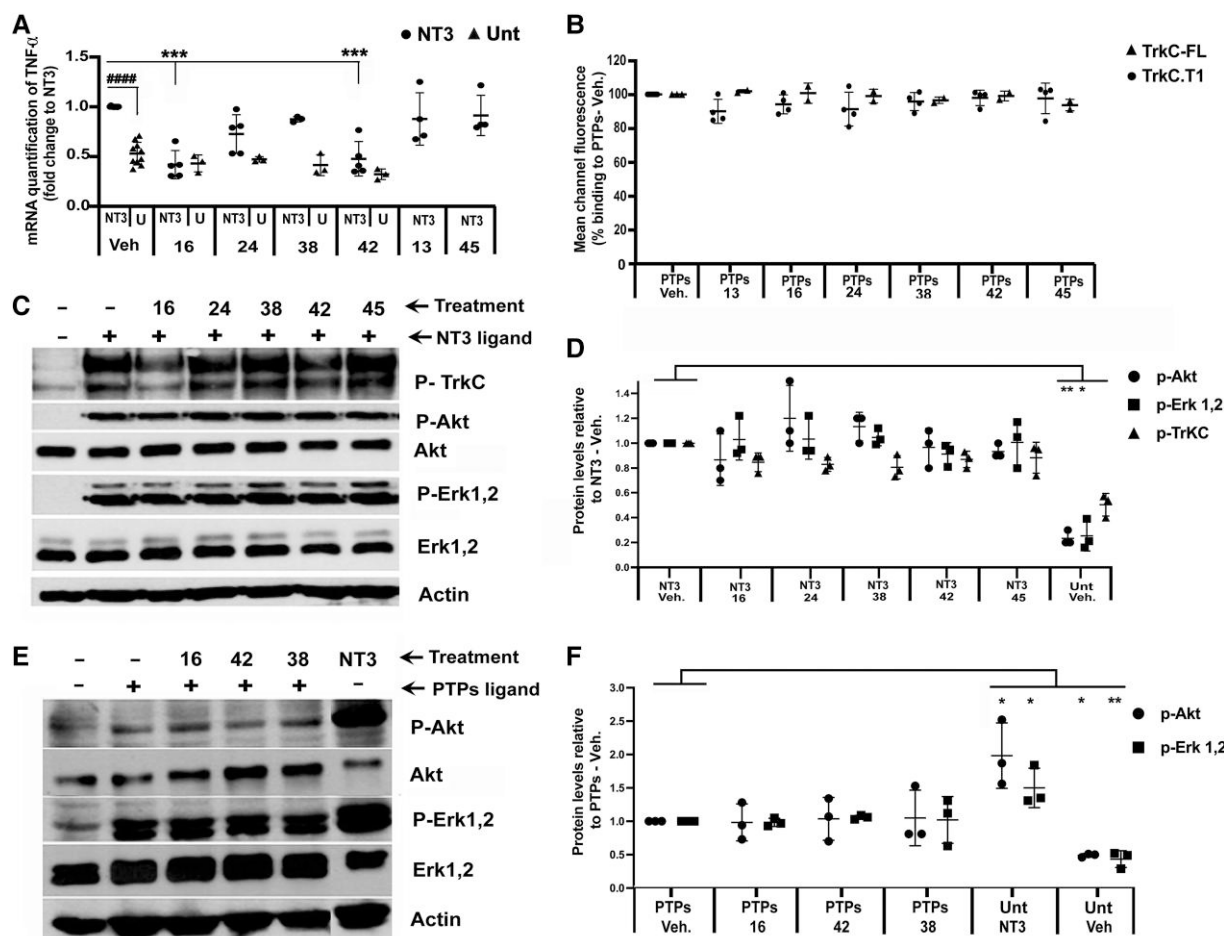
Fig. 4. Agents 16 and 42, analogs of **2d'**, are selective TrkC.T1 antagonists biased to inhibiting NT3-promoted activation. A) Sixteen and 42 inhibit TrkC.T1-mediated TNF-α up-regulation induced by NT3. TNF-α transcripts were quantified by real-time PCR of TrkC.T1-expressing cells after 6 h in the presence of NT3 as indicated or without NT3 (U or Untreated). Values are standardized to vehicle (Veh) + NT3 treatment = 1. Each condition (±NT3) was treated with Veh control or with the indicated agent. Data are the mean ± SD of at least three independent experiments, each independent assay done in triplicate wells. NT3-treated cells have significantly higher TNF-α mRNA compared with untreated cells (####$P < 0.0001$). NT3-Veh has significantly higher TNF-α mRNA compared with NT3+ test agents **16** or **42** (***$P < 0.001$, ****$P < 0.0001$). One-way ANOVA with significance $\alpha < 0.05$ followed by Bonferroni's correction for multicomparisons. Other statistical differences are omitted in the graph for clarity. B) Analogs do not block PTPs-Fc binding to TrkC.T1 or to TrkC-FL. Cells expressing TrkC.T1 or TrkC-FL were preincubated ± the indicated agents (10 µM) followed by addition of PTPs-Fc (40 nM). Cells were analyzed by flow cytometry. MFC of PTPs-Fc + Veh control is standardized to 100% binding. Values are the mean ± SD of three independent experiments each acquiring 10,000 cells. C) Analogs do not block NT3•TrkC-FL signal transduction. TrkC-FL-expressing cells were exposed to the indicated agents (10 µM) ± NT3 (0.2 nM), and detergent lysates were analyzed by western blotting with antibodies directed to phospho-MAPK, phospho-Akt, and for standard loading control total actin, total Erk1,2, or total Akt. Data are quantified in D. D) Densitometric quantification of *P*-TrkC, p-Erk1,2, and p-Akt induced by NT3 in TrkC-FL cells. Data are expressed as the ±SD, relative to NT3 (100%), in at least three independent experiments. Statistics were calculated by one-way ANOVA with significance $\alpha < 0.05$ followed by Bonferroni's correction for multicomparisons. Symbols indicate significantly lower activation of phospho-Erk1,2 and phospho-Akt in untreated Veh control compared with Veh + NT3 (*$P < 0.05$, **$P < 0.01$). The agents did not impact on NT-3 stimulation of phospho-TrkC, phospho-Erk1,2, and phospho-Akt. E) Analogs do not block PTPs•TrkC-FL signal transduction. TrkC-FL-expressing cells were exposed to the indicated agents (10 µM) ± PTPs (40 nM), and detergent lysates were analyzed by western blotting with antibodies directed to phospho-MAPK, phospho-Akt, and for standard loading control total actin, total Erk1,2, or total Akt. Data are quantified in F. F) Densitometric quantification of p-Erk1,2, and p-Akt induced by PTPs in TrkC-FL cells. Data are expressed as the mean ± SD, relative to PTPs (100%), in at least three independent experiments. Statistics were calculated by one-way ANOVA with significance $\alpha < 0.05$ followed by Bonferroni's correction for multicomparisons. Symbols indicate differences with respect to Veh + PTPs (*$P < 0.05$, **$P < 0.01$). Veh control has significantly lower activation than PTPs treatment. NT3-treated cells have significantly higher activation of phospho-Erk1,2 and phospho-Akt compared with PTPs treatment, as reported. The agents did not impact on PTPs stimulation of phospho-Erk1,2 and phospho-Akt.

AlphaFold3, a machine-learning and diffusion-based algorithm for high-accuracy prediction of biomolecular structures (25). The structure of the isolated TrkC shows that the ECD is folded, with the LRR-like and D4–D5 subdomains displaying restricted motions, as indicated by the low position error between the subdomains (Fig. S4A and B). Next, we modeled the complex of TrkC with the ligands NT3 and PTPRS. NT3 forms a dimer nearly identical to the crystal structure (e.g. PDB 1B8K) (26, 27) and binds two copies of TrkC via the D5 domain, while PTPRS binds the

LRR-like subdomain, as expected (Fig. S4C and D). Next, the predicted TrkC and TrkC–NT3–PTPRS structures were used to model interactions with the small molecule **CP14** using molecular docking. **CP14** docked preferentially on the D5 subdomain, adjacent to the NT3-docking site in both structures (Fig. S4E and F). The docking prediction is consistent with the NT3 bias of **CP14**, because PTPs bind at the LRR subdomain near the ectodomain N-termini (see Fig. S4C), and it is also consistent with the experimental finding suggesting that **CP14** lowers NT3 affinity in a noncompetitive
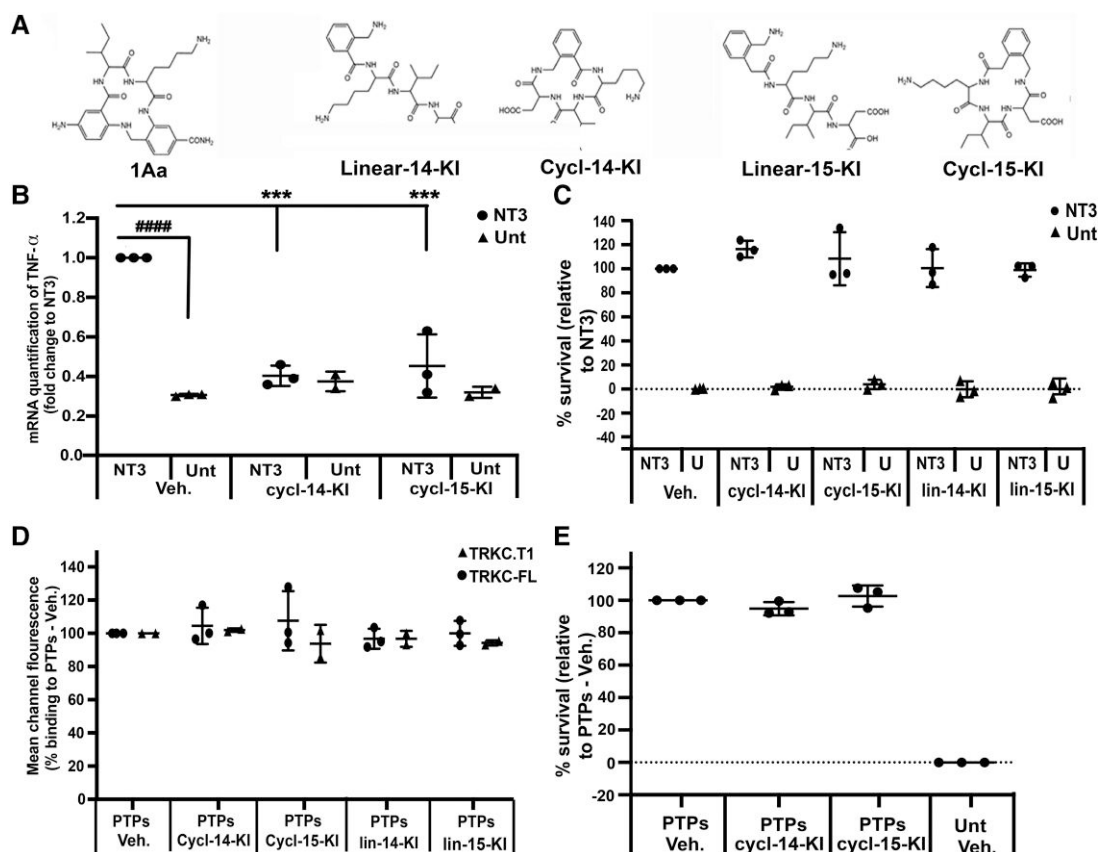
Fig. 5. Converting a TrkC-FL agonist 1Aa into a TrkC.T1 antagonist. A) Structure of **1Aa**, and analogs **cyclic-14-KI (CP14)**, **cyclic-15-KI (CP15)**, and their corresponding unstructured linear forms as controls. B) **CP14** and **CP15** inhibit NT3-induced up-regulation of TNF-α mRNA in TrkC.T1-expressing cells. Real-time qPCR quantification of TNF-α mRNA after 6 h of the indicated treatment. The values were standardized to vehicle (Veh) + NT3 control treatment (=1 or 100%). Data are the mean ± SD of at least three independent experiments, each assay in triplicate wells. One-way ANOVA with significance α < 0.05 followed by Bonferroni's correction for multicomparisons. In the absence of agents, NT3-treated cells are significantly higher compared with Veh-treated cells (####$P < 0.0001$). Agents **cyclic-14-KI (CP14)**, **cyclic-15-KI (CP15)** significantly reduce NT3-promoted TNF-α mRNA (***$P < 0.001$), to levels equal to untreated baseline. In the absence of NT3, the agents have no effect. Other statistical differences are not indicated in the graph, for clarity. C) Agents (active cyclic or control linear) do not impact on NT3-induced survival of TrkC-FL-expressing cells cultured in SFM. Cells were supplemented ± the indicated agents (10 µM) or Veh ± NT3 (0.2 nM), a concentration of NT3 which affords low but significant survival. This condition was selected as it is easier to detect inhibition or toxicity. Data are standardized to Veh + NT3. Shown are the ±SD of at least three independent experiments, each assay in triplicate wells. D) Analogs (active cyclic or control linear) do not block binding of PTPs-Fc to TrkC-FL or to TrkC.T1 receptors. Cells expressing TrkC-FL or TrkC.T1 were preincubated with the indicated agents (10 µM), and the binding of PTPs-Fc (40 nM) was quantified by flow cytometry. MCF values of Veh + PTPs control are set to 100% binding. Shown are the mean ± SD of at least three independent experiments. E) Analogs (active cyclic) do not inhibit PTPs-induced survival of TrkC-FL-expressing cells in serum-free cultures. Cells were supplemented ± the indicated agents (10 µM) or Veh ± PTPs (40 nM). Data were standardized to Veh + PTPs. Shown are the mean + SD of at least three independent experiments, each assay in triplicate wells.

Table 3. CP14 reduces the affinity of NT3 for TrkC.T1.

Competitor	µM	K_d NT3 (nM)	
		TrkC.T1	TrkC-FL
Veh	0	1.8	3.6
Compound **16**	1	1.4	3.9
	5	3.0	4.0
	15	3.2	3.6
CP14	1	6.1	4.0
	5	7.4	3.7
	15	11.5	4.1

A dose range of cyclic-14-KI (**CP14**) or compound **16** was tested vs. a dose range of NT3-bio as described in Materials and methods. The K_d of NT3 for each TrkC isoform (±antagonist) was determined from the binding constants measured at different antagonist:ligand stoichiometries. Examples of raw binding data are shown in Fig. S4.

allosteric manner. Additional work and an experimentally accurate 3D model of TrkC.T1 as monomer or as a homodimer would be required to confirm this.

Therapeutic efficacy of TrkC.T1 antagonists in a model of RP

For testing therapeutic efficacy in vivo in the RHOP347S transgenic mouse model of RP, we selected compound **16** from the first chemical biology approach and **CP14** from the second chemical biology approach. The RHOP347S mice recapitulate an aggressive form of human RP by transgenic expression of a *rhodopsin* gene mutation. In RHOP347S transgenic mice (but not in wild-type [WT] mice), TrkC.T1 and NT3 are significantly up-regulated in Müller glia shortly after the mice open their eyelids at postnatal day 15 (PN 15) and retinas are exposed to light, causing increased TNF-α production, and photoreceptor neuronal death. RHOP347S mice suffer ~50% photoreceptor death by PN 18, and nearly total photoreceptor loss by PN 28 (28). We have reported that in this mouse model a knockout of one TrkC.T1 allele or the silencing of the TrkC.T1 mRNA normalizes TNF-α production and reduces photoreceptor death (15). Hence, we investigated whether small molecule TrkC.T1 antagonists would yield comparable therapeutic results.

Initially, we used explanted organotypic cultures of retinas obtained from PN 18 RHOP347S transgenic mice or from control WT mice. The photoreceptors of RHOP347S retinal explants recapitulate neurodegeneration with the same kinetics as in vivo, whereas WT retinas remain healthy within the time frame of the experiment (15, 29). Retinal TNF-α protein was quantified by western blots, and the death of photoreceptors was quantified by confocal microscopy of TUNEL+ staining of the photoreceptor layer (Fig. 6).
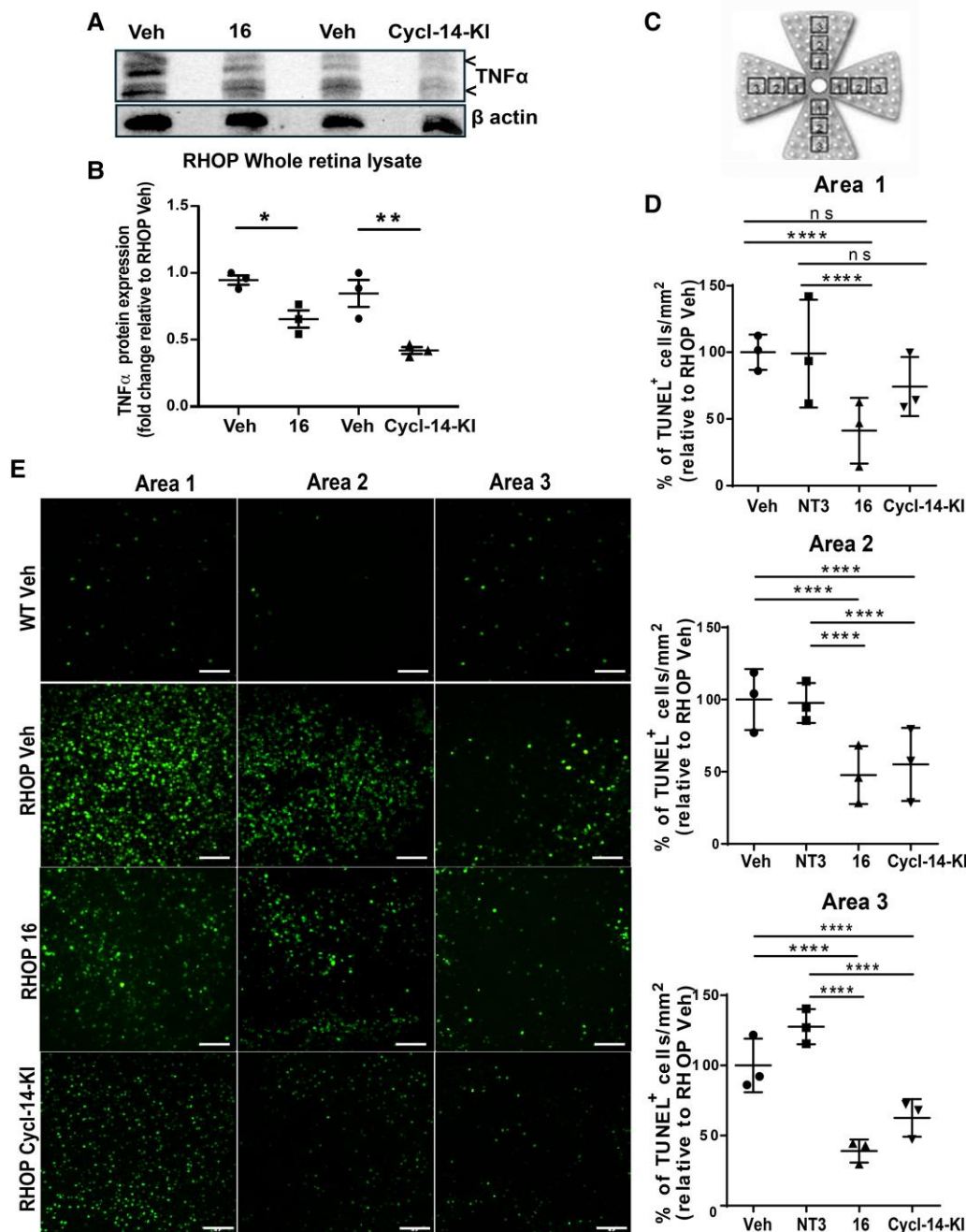

Fig. 6. TrkC.T1 antagonists decrease TNF-α protein and cell death in retinal explants of RHOP347S mice. RHOP347S retinas were cultured for 24 h in the presence of TrkC.T1 antagonists as indicated (agent **16**), or **cyclic-14-KI** (CP14) (20 μM) or with vehicle (Veh) control, or NT3 as control (20 nM). A, B) PN day 18 RHOP347S retinas were cultured as organotypic explants and treated for 24 h with Veh control, or with antagonists **16** or **CP14**. TNF-α protein (arrows show the membrane and soluble TNF-α) was quantified in western blots of lysates from whole retinal tissue. One-way ANOVA with significance $\alpha < 0.05$ followed by Bonferroni's correction for multicomparisons show significantly reduced TNF-α after treatment with agents **16** (*$P < 0.05$) or **CP14** (**$P < 0.01$); $n = 4$ independent experiments ± SD, after normalization to β-actin loading control in each corresponding experiment. C) Pictogram depicting the geography of areas 1, 2, 3 of the retina, to account for the natural thinning of the photoreceptor layer (which is thicker in center and thinner in periphery). D). For each retina ($n = 3$ retinas per group), one picture was taken per each area for each quadrant (12 pictures total per retina). TUNEL+ photoreceptors were counted semi-automatically (ImageJ). Quantified data are shown as the mean ± SD for each concentric area of the retina (****$P < 0.0001$, **$P < 0.01$, *$P < 0.05$). One-way ANOVA with significance $\alpha < 0.05$ followed by Bonferroni's correction for multicomparisons. Data show significantly reduced photoreceptor death when comparing controls Veh or NT3 vs. TrkC.T1 antagonists **16** or **CP14**. All areas have significantly lower photoreceptor death compared with controls (****$P < 0.0001$), except for area 1 where **CP14** treatment is not significant (ns). E) Representative pictures for each retinal area ($n = 12$ pictures per area) showing TUNEL+ photoreceptors. Organotypic cultures of RHOP347S retinas in culture for 24 h exhibit apoptosis, and treatment reduced the TUNEL+ nuclei. Control organotypic cultures of WT retinas do not show apoptosis.

Treatment of RHOP347S organotypic retinal cultures with TrkC.T1 antagonists **16** and **CP14** significantly reduced TNF-α protein levels (Fig. 6A, quantified in Fig. 6B) and significantly decreased photoreceptor death across all areas of the retina (quantified in Fig. 6D), when compared with the control vehicle-treated RHOP347S organotypic retinas. There are no statistical differences in efficacy between antagonists **16** and **CP14** in either bioassay. Control treatment with exogenous NT3 (20 nM) did not impact positively or negatively on TUNEL+ counts. This was expected because NT3 is already significantly up-regulated in RHOP347S retinas (15, 30). Control organotypic retinal cultures from healthy WT mice (without significant TUNEL+ counts) treated ± antagonists **16** or **CP14** shows no affect in TUNEL+ counts. Hence, the antagonists do not impact positively or negatively healthy retinas that do not have detectable TrkC.T1. Representative pictures of TUNEL+ images in the photoreceptor layer are shown (Fig. 6E). Data are shown separately for each retinal area concentric to the optic nerve head, to account for the architecture of the retina (thicker in the central area; and thinner in the periphery, see Fig. 6C).

Based on the data resulting from organotypic culture assays, we next tested antagonists in vivo. RHOP347S mice at PN day 18 (a time point where there is already photoreceptor damage) were treated by intravitreal injection of either **16** or **CP14** in one eye, and control vehicle in the contralateral eye. In this experimental paradigm, each mouse has its own internal control, which reduces mouse-to-mouse variability.

Two days after intravitreal injections, the retinas were processed for TUNEL+ and counts in the photoreceptor layer were quantified by area to account for the natural thinning of the retinal architecture (thicker in the central area; and thinner in the periphery, see Fig. 6C). Compounds **16** or **CP14** significantly reduce photoreceptor death in areas 1 and 2 of the RHOP347S retina (Fig. 7A).

Quantification of photoreceptor nuclei represents surviving photoreceptors and is another way to evaluate reduced photoreceptor death. RHOP347S eyes treated with **CP14** or compound **16** have significantly more surviving photoreceptors when compared with vehicle (Fig. 7B). Moreover, the thickness of the photoreceptor layer showed a significant preservation of the outer nuclear layer (ONL) structure in the drug-treated RHOP347S eyes when compared with vehicle-treated RHOP347S eyes (Fig. 7C). These data are with the interpretation of increased surviving photoreceptors and preservation of the structure of the ONL retinal layer where photoreceptor cell bodies reside.

Together, the data are consistent in showing reduced photoreceptor death, increased numbers of photoreceptor nuclei, and increased photoreceptor layer thickness and preservation of structures by treatment of RHOP347S mice in vivo with compound **16** or with **CP14**. We note that compared with WT retinas, the drug-treated RHOP347S retinas had significantly lower photoreceptor counts and ONL thickness. This was expected, because therapy was initiated at PN 18 and retinas were analyzed at PN 20; a stage when there is preexisting ~40% photoreceptor loss in RHOP347S retinas (15, 16) which treatment does not regenerate.

Discussion

We used two chemical biology approaches to analog reported nonselective TrkC antagonists (20–23) and reported TrkC agonists (17, 31). Screening identified selective antagonists of NT3•TrkC.T1, that do not inhibit PTPs•TrkC.T1 and that do not inhibit prosurvival signals by NT3•TrkC-FL or PTPs•TrkC-FL.

Receptor selectivity and ligand bias

Some of the agents (**16** and **42**; **CP14** and **CP15**) selectively antagonize TrkC.T1•NT3 by reducing ligand affinity in an allosteric manner, but do not impact on PTPs binding to TrkC.T1, and do not affect TrkC-FL activation by either NT3 or PTPs, or the function of other Trk-receptor family members. Hence, the agents are biased antagonists of NT3•TrkC.T1 (see summary in Table 2).

With regards to mechanisms, analyses of the NT3-binding constants demonstrated that **CP14** reduces the affinity for TrkC.T1 but not for TrkC-FL; and the data also suggest an allosteric noncompetitive mechanism. Modeling and docking predictions also suggest an allosteric mode of binding for **CP14** at the D4–D5 interface of TrkC.T1. We note, however, that a fundamental limitation of AlphaFold is that it cannot capture alternative or multiple low-energy conformations that could results from different disulfide bonding patterns. As expected, the AlphaFold-model of the receptor structure is identical between TrkC-FL and TrkC.T1, because the sequence of the extracellular region is identical; yet, the structures of the ectodomains differ as we reported that their disulfide bonding pattern differs as TrkC.T1 disulfides are rearranged by Protein Disulfide Isomerase enzymes (11). Additional work and an experimentally accurate 3D model of TrkC.T1 would be required to confirm that **CP14** binds at this site, but the modeling at least suggests that it is plausible for our small molecules to bind TrkC and affect the interaction with the NT3 ligand.

Therapeutic efficacy in RP

The etiology of glial-derived TNF-α in many degenerative retinal dystrophies is well-known (32, 33). Intravitreal injection of anti-TNF-α mAb delays retinal degeneration in RP (34) and in other retinal dystrophies where TrkC.T1 is up-regulated in glia [e.g. glaucoma (6, 35, 36)]. For this reason, we posit that modulating a target receptor that induces TNF-α, such as TrkC.T1, may be relevant therapeutically in many pathologies.

In a genetic mouse model of RP where TrkC.T1 is up-regulated at the onset of disease (15, 16), two TrkC.T1 selective antagonists **16** and **CP14** were applied therapeutically 1× after disease onset. The agents prevent TNF-α up-regulation and reduce photoreceptor neuronal death in vivo. These data validate TrkC.T1 as a therapeutic target and demonstrate the efficacy of an antineurotoxic strategy that results in neuroprotection.

TrkC.T1 is a naturally occurring receptor isoform that is significantly up-regulated in RP (degeneration of photoreceptors) and other neurodegenerative diseases, such as glaucoma (degeneration or retinal ganglion cells) (30), ALS (degeneration of motor neurons) (10, 15), and noise-induced neurosensory hearing loss (degeneration of inner ear neurons) (2) (7, 37–39), and in some types of cancer (40, 41). The pharmacological efficacy of TrkC.T1 inhibition in a model of RP suggests possible therapeutic options to ameliorate pathologies in these other diseases.

The efficacy of TrkC.T1 antagonists is statistically significant, and comparable with other reported experimental or applied approaches such as vitamin and nutritional supplementation (beneficial but only for a limited group of patients). This is important especially considering the early onset and rapid progression of the transgenic mouse model of RP evaluated in our work, and the fact that TrkC.T1 antagonists were applied only once in challenging therapeutic paradigms, after onset of disease and with ongoing inflammation and neurodegeneration. As comparison, gene therapy (voretigene neparvovec) specific for the RPE65 mutation causing Leber congenital amaurosis received approval from the
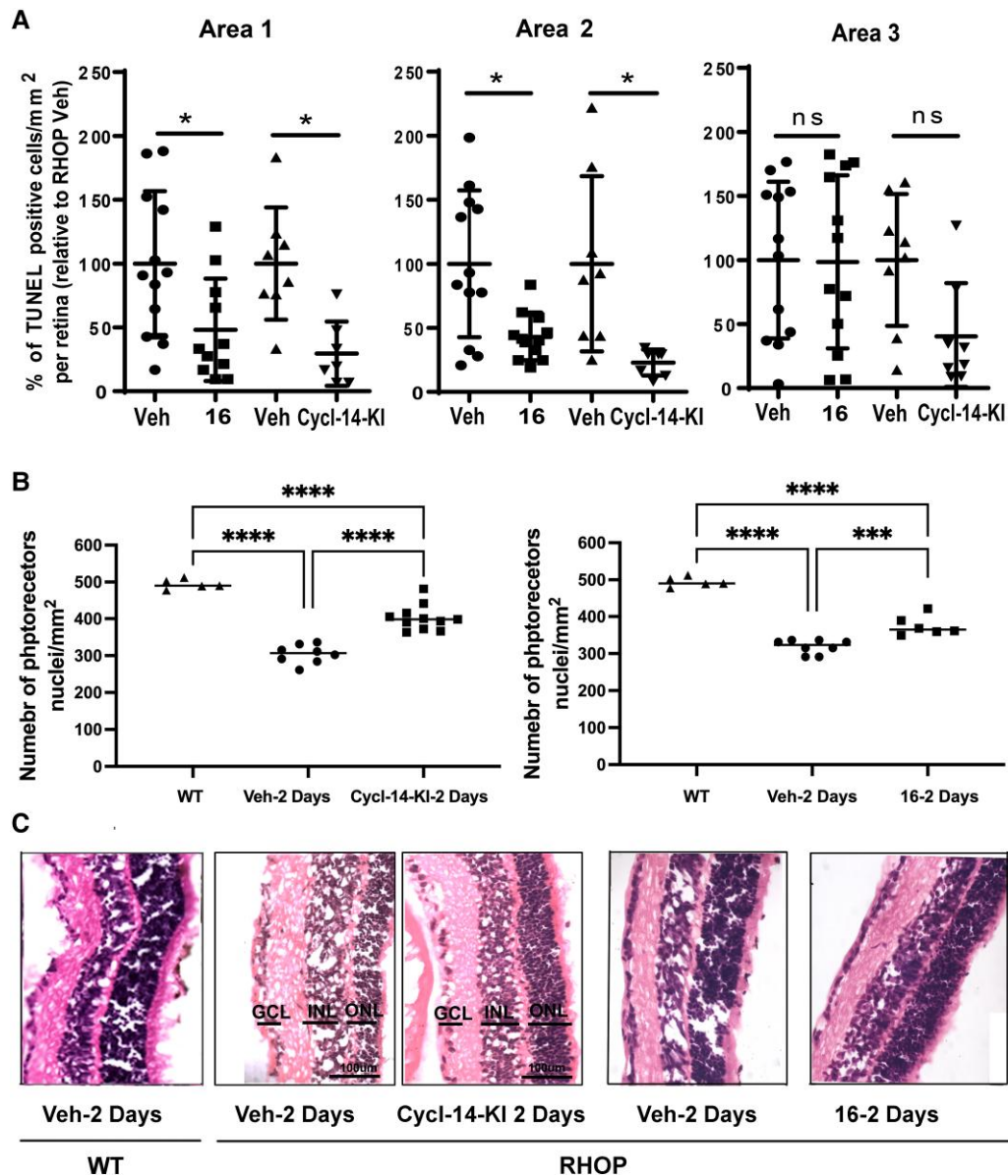
Fig. 7. Agents 16 and cyclic-14-KI (CP14) decrease photoreceptor cell death in the RHOP347S mice retina in vivo. WT or RHOP347S transgenic mice at PN day 18 were injected intravitreally with either vehicle (Veh) control (physiological saline) or with **16** or with **CP14**. At PN 20 (e.g. 2 days after injections), eyes were enucleated and whole mount retinas were prepared for quantification of photoreceptor death (TUNEL$^+$ photoreceptors) or for quantification of surviving photoreceptors (counting photoreceptor nuclei) in stained sections. A) Quantification of TUNEL$^+$ nuclei shows significantly reduced photoreceptor death when comparing Veh-treated eye (left) of each mouse to the contralateral eye (right eye) treated with TrkC.T1 antagonists **16** ($n = 12$) or **CP14** ($n = 8$). Only areas 1 and 2 are significant (*$P < 0.05$). One-way ANOVA with significance $\alpha < 0.05$ followed by Bonferroni's correction for multicomparisons. B) Quantification of photoreceptor nuclei of the INL and ONL layers, in H&E-stained sections of RHOP347S transgenic mice treated with Veh or **CP14**. For quantification, $n = 8$–16 images were taken under 40× magnification from areas 1 and 2. One-way ANOVA with significance $\alpha < 0.05$ followed by Bonferroni's correction for multicomparisons. Data show a significant increase in the number of live photoreceptors after **CP14** treatment when compared with Veh (****$P < 0.0001$). C) Representative brightfield images of H&E-stained sections (quantified in B). Scale bar = 100 µm. The photoreceptor cells are stained dark (color purple). GCL ganglion cell layer, INL inner nuclear layer, ONL outer nuclear layer. Note that images compare the left eye (Veh) to the right eye (test agent) in each mouse, so in most cases each mouse has its own internal control that reduces mouse-to-mouse variability. Hence, when sections are prepared from the same area (Fig. 6C) changes are evident only in the thickness and staining intensity of the ONL (where photoreceptors are), while the GCL and INL of both eyes are of equal thickness and staining intensity.

FDA. However, hundreds of mutations are reported in the Rhodopsin gene and other genes of the visual system that can lead to RP or neuronal degeneration, making gene therapy approaches a one-at-a-time and a mutation specific.

Since TrkC.T1 is expressed in many forms of retinal dystrophies and it is etiological to inflammatory pathways upstream of the well-known target TNF-α, the TrkC.T1 target may offer therapeutic opportunities for larger patient populations. The TrkC.T1 antagonists may be effective in the retina due to a small volume of distribution and slow clearance of the vitreous; and in future work, we will test them in other sites such as intrathecally in the spinal cord in ALS.

The TrkC.T1 antagonists reported here have potential for medical translation, because they are small molecules (range 500–1,200 Da) chemically and structurally related to small molecules that have proven safe, suitable, and effective for therapy of retinal diseases (42–46) or for the experimental therapy of brain diseases requiring CNS penetration (47–50).

Chemical biology strategies for developing TrkC.T1 small molecule antagonists

Small molecule inhibitors were identified using two different chemical biology approaches combined with screening for effects on NT3•TrkC.T1, and lack of effects on NT3•TrkC-FL or PTPs•TrkC-FL, as well as lack of effect on Trk-receptor family members.

In the first approach, known antagonists of TrkC-FL were reevaluated, to yield compound **2d'** (RI-TG) as a TrkC antagonist that is not isoform specific. Two analogs of **2d'**, agents **16** (KE-GT) and **42** (TG-IR), are specific antagonists of TrkC.T1, biased to antagonizing NT3•TrkC.T1 without inhibiting PTPs•TrkC.T1 binding; and not impacting NT3•TrkC-FL or PTPs•TrkC-FL activation.

A comparison of nonisoform-selective **2d'** (RI-TG) to the isoform-selective TrkC.T1 antagonist **42** (TG-IR) suggests that sequence inversion enables target specificity, at least with regards to NT3-dependent events. Consistent with this notion, related agents **2c'** (**GT-EK**) and **2e' (SM-GK)** antagonize NT3•TrkC-FL (also see Ref. (17)). The relevance of bivalency in these agents is shown by the fact that the monomers do not have antagonistic activity against any isoform. These results support the concept that it is possible to convert a nonselective TrkC ligand into a selective TrkC.T1 antagonist. Perhaps this strategy may be used for related scenarios or for making analogs of other small molecule ligands, though the strategy is of course not expected to be universal.

In the second approach, we converted a small molecule agonist of TrkC, **1Aa**, into a selective TrkC.T1 antagonist. The analogs **CP14** and **CP15** significantly blocked the NT3•TrkC.T1-induced up-regulation of TNF-α, with no impact on other parameters. The importance of a β-turn displaying the IK pharmacophore is demonstrated because these agents are antagonists only in their cyclic (β-turn) configuration but are not antagonists in their linear or unstructured forms. The binding and the biological data are summarized in Table 2.

The chemical biology approaches we used for developing selective TrkC.T1 antagonists may be useful also for targeting other receptor families, where isoforms, mutations, or posttranslational modifications create an opportunity to exploit selectivity.

Conclusions

Our results support the concept that accounting for the functional and the structural heterogeneity of receptor–ligand interactions is useful to validate novel therapeutic targets and to enable new pharmacological strategies. In future work, we will explore combining the complementary approaches of direct promotion of neuronal survival by activating TrkC-FL in neurons, together with reduction of the neurotoxicity induced by glial TrkC.T1; aiming to achieve optimal neuroprotection.

Materials and methods
Cell lines

HEK 293 or NIH3T3 cells were transfected with plasmids encoding human full-length *TrkC* (293-TrkC-FL and NIH-TrkC-FL) or with human or rat TrkC.T1 (293-rTrkC.T1, 293-hTrkC.T1, and NIH-TrkC-T1). The rat Müller glial cell line rMC-1 (51) was transfected with plasmids encoding human TrkC.T1 (rMC-1-TrkC.T1). Stably transfected subclones that express TrkC-FL or TrkC.T1 receptors were drug selected (depending on the vector, 0.5 mg/mL G418, 2 μg/mL puromycin, or 10 μg/mL blasticidin). Expression was verified by qPCR using specific primers of each isoform (10), by flow cytometry, by IHC, and by western blots using our own in-house mAbs 2B7 (52), 1E11 (11), the mAb TrkC 1 (2), and a commercial mAb C44H5 antibody (catalog 3376; Cell Signaling). The mAb 2B7 binds only to TrkC-FL at the IgG-C2 (D5) domain (52) at an epitope conserved in mouse, rat, and human TrkC-FL. The mAb TrkC 1 binds to both TrkC-FL and TrkC.T1 (2). The mAb 1E11 is selective for TrkC.T1 ectodomain (11). For western blots, anti-p-ERK1/2 (catalog 4377S; Cell Signaling), anti-phospho-Akt (catalog 4060S; Cell Signaling), anti-actin (catalog A5316; Sigma), and anti-TNF-α (catalog 500-P64; PeproTech) were purchased.

Protein receptor ligands

NGF, BDNF, and NT3 growth factors were purchased (Alomone Labs and ProSpec-Tany). Biotinylated NT3 was prepared using Sulfo-NHS-LC-Biotin (Thermo Fisher Scientific) by incubation of 2 μM of NT3 with 400 μM of Sulfo-NHS-LC-Biotin for 40 min at room temperature in PBS (20-fold molar excess of biotin reagent). Biotinylated NT3 was concentrated, and unbound biotin was removed, using a desalting Amicon Ultra-0.5 mL centrifugal filter (Ultracell: 10 kDa; Millipore). PTPs soluble ectodomain protein fused to IgG-Fc was prepared, as described previously (13).

Synthesis and characterization of small molecules

The synthesis, purification, and characterization were reported (17, 20, 22, 31). For direct binding assays to receptor isoforms, the TrkC-FL antagonists **2c'**, **2d'**, and **2e'** were tagged with biotin, and analogs were tagged with polyethylene glycol as described (17). **1Aa** is a reported TrkC agonist (20), and analogs were screened to find antagonists. The **1Aa** analogs were synthesized as cyclic agents to mimic a β-turn conformation of neurotrophins, and as controls their linear (unstructured) forms were prepared as well. Synthesis started with a linear peptide (K-I-D) assembled on Asp(Wang resin)-OAll (loaded 0.51 mmol/g; Novabiochem) on a reaction using Fmoc-coupling chemistry, and deprotection was performed with 20% piperidine in DMF. To avoid incomplete reactions, the couplings and deprotections were repeated twice at each step. The attachment to AMPA, respectively ABMA, was done with a TBTU, followed by a HBTU as a coupling reagent. The Allyl protecting group of the Asp was removed after treatment with Pd (PPh$_3$)$_4$/PhSiH$_3$. The head-to-tail cyclization of the linear peptide-resin was performed with double coupling with HATU (in the case of a 14-membered ring peptide) or with PyBOP (in the case of a 15-membered cycle). The peptides were cleaved and removed from the resin by incubation in 95% trifluoroacetic acid at RT with agitation for 2.5 h. Purification was done with Varian high-pressure liquid chromatography (HPLC) apparatus and a Chromasil C18 reverse-phase column (10 × 250 mm). Buffer A was 10% ACN in water with 0.1% TFA and buffer B was 70% acetonitrile with 0.1% TFA. Gradient was buffer B from 0 to 40% in 20 min with a 3.5 mL/min flow rate. HPLC analysis of the pure peptides was done with a Phenomenex C18 reverse-phase column (4.6 × 75 mm) with similar buffers, but a gradient from 0 to 100% B in 10 min and a 0.1 mL/min flow rate.

Electrospray mass spectrometry (positive mode) was carried out with a Thermo Q Exactive at a resolution of 35,000, which confirmed the expected masses. Cyclic peptide AMBA-14-KID: MS-direct infusion (ESI): m/z [M + H]$^+$ calculated for C$_{24}$H$_{36}$N$_5$O$_6$, 490.259; found 490.260. Cyclic peptide AMPA-15-KID: FTMS (ESI, +mode): m/z [M + H]$^+$ calculated for C$_{25}$H$_{38}$N$_5$O$_6$, 504.274, found 504.281. Cyclic peptide AVA-15-OID: MS-direct infusion (ESI): m/z [M + H]$^+$ calculated for C$_{20}$H$_{36}$N$_5$O$_6$, 441.266, found 442.265. Linear peptide AMBA-14-KID: MS-direct infusion (ESI): m/z

$[M + H]^+$ calculated for $C_{24}H_{38}N_5O_7$, 508.269, found 508.270. Linear peptide AMPA-15-KID: MS-direct infusion (ESI): m/z: $[M + H]^+$ calculated for $C_{25}H_{40}N_5O_7$, 522.285, found 522.293.

Dimers on a triazole core

Bivalent analogs in a triazole core were assembled with different orientation and sequences, as described previously (17, 20–22). Combinations were prepared in three different sets. Set **1** (forward only): R^1R^2 and $R^3R^4 = i+1-i+2$ and $i+1-i+2$, e.g. TG-TG, set **2** (opposite only): R^1R^2 and $R^3R^4 = i+2-i+1$ and $i+2-i+1$, e.g. GT-GT, and set **3** (forward-opposite): R^1R^2 and $R^3R^4 = i+1-i+2$ and $i+2-i+1$, e.g. TG-GT. In silico evaluation of the small molecules using the Pan Assay Interference Compounds program (53) showed no concerns.

Direct TrkC-binding assays using biotin-conjugated small molecules

Agents were tested by quantitative flow cytometry assays (52). Briefly, WT HEK293 or WT NIH, or their transfected counterparts expressing stable TrkC-FL or TrkC.T1 was resuspended in binding buffer (PBS, 0.2% bovine serum albumin [BSA], 0.1% Na Azide) and incubated with 10 µM of the indicated biotinylated agents for 30 min at 4 °C. Cells were washed in cold binding buffer, and exposed to secondary agent fluorothiocyanate-labeled avidin (avidin-FITC, catalog: A 2050; Sigma) for 20 min at 4 °C. After washing two times in binding buffer, cells were analyzed immediately by flow cytometry (Fortessa) and FlowJo software. The mean channel florescence values of WT cells (not expressing any TrkC) were standardized to 1 for each experiment, and data shown are the mean ± SD of at least three independent experiments.

Competition assays to block binding of PTPs or anti-TrkC mAb to TrkC

Agents were assayed by quantitative flow cytometry (52) for their ability to compete the binding of a PTPs-receptor-body containing PTPs-ectodomain linked to a human antibody Fc domain (PTPs-Fc) (11) or to compete the binding of anti-TrkC mAb TrkC 1 (2) that binds to both isoforms.

Cells were incubated ± the indicated agents (10 µM) or vehicle control for 20 min at 4 °C in binding buffer, followed by addition of saturating concentrations of primary reagent: PTPs-Fc (40 nM) or TrkC 1 mAb (67 nM). After incubating for 20 min, cells were washed, and resuspended for 20 min at 4 °C in binding buffer with the proper secondary antibodies with a fluorescent label (F9512; Sigma). After two washing steps, cells were resuspended in binding buffer and data were acquired immediately by flow cytometry and analyzed using FlowJo software. For negative staining controls, the primary reagent was omitted (background fluorescence). For cellular and receptor specificity controls, WT cells or cells expressing TrkC-FL or TrkC.T1 receptors were analyzed. The mean channel fluorescent (MFC) values of vehicle control treatment (no competition) are standardized as 100% binding. Data are the mean ± SD of at least three independent experiments.

Competition assay to block binding of NT3

Competition of NT3-biotin binding to TrkC isoforms was performed, as described previously (11, 52) using compound **16** or **Cyclic-14-KI**, or "cold NT3" (not biotinylated) as a positive control for self-competition. Cells in binding buffer (PBS + 0.2% BSA + 0.1% Na Azide) were treated with a concentration range (0–1–5–15 µM) of compound **16** or Cyclic-14-KI. Then, a concentration range of

NT3-biotin (0–40 nM) was added to each concentration of test compound, with a 15-min incubation at 4 °C. After washing in ice-cold binding buffer, cells were treated with the secondary reagent conjugated avidin-fluorescein (Sigma) for 15 min at 4 °C. After two washing steps, live cells were analyzed immediately by flow cytometry. Analysis in GraphPad was performed to determine the K_d of NT3•TrkC and the mode of NT3•TrkC-binding inhibition (allosteric, noncompetitive, or competitive).

Cell metabolism/survival

The growth/survival profile of the cells was quantified in 96-well plates using the tetrazolium salt reagent 4-[4,5-dimethylthiazol-2-yl]-2,5-diphenyltetrazolium bromide (MTT; Sigma) 48 h after plating; by reading the optical density, as previously described (54). Cells cultured in serum-free medium (SFM) die by apoptosis, but they can be rescued if they express TrkC-FL and are supplemented with NT3 or PTPs. Wells received vehicle control or were supplemented ± NT3 or PTPs (cognate agonists) ± test agents at the indicated concentrations.

Studies in the absence of NT3 or PTPs or NT3 assess the possibility of (partial) agonism (limited survival) and whether agents cause toxicity (accelerated death). Studies in the presence of NT3 or PTPs respectively at their optimal (2 and 40 nM) and suboptimal (0.2 and 8 nM) concentrations (11) assess the pharmacological mechanism of (partial) antagonism, or (partial) agonism. Specificity cellular controls used cells expressing receptor family members TrkA or receptor TrkB, treated with respective positive controls NGF or BDNF. Assays were repeated $n \geq 3$ independent times, each independent assay in quadruplicate. MTT data are standardized to optimal dose of neurotrophin = 100% survival, and SFM = 0% survival, using the formula $[(OD_{test} - OD_{SFM}) \times 100/(OD_{optimal\ NTF} - OD_{SFM})]$.

Quantification of TNF-α mRNA

rMC-1 cells expressing human TrkC.T1 were treated as indicated for 6 h, with or without NT3 (2 nM) and with or without test agents (10 µM). Quantification of TNF-α mRNA was performed by real-time quantitative PCR and primers used for rat TNF-α and rat RNAs18 reported (10). The values (relative changes in mRNA expression levels) were standardized to the positive control NT3. Data are the mean of at least three independent experiments ± SD, each in triplicate.

Signal transduction assays

The activation of signaling proteins Trk, Akt, and Erk1,2 was studied by western blotting of their phosphorylated states relative to the total Trk, Akt, Erk1,2 proteins, and standardized to actin control. NIH-TrkC-FL cells were cultured in SFM for 120 min (to reduce background and serum signals) and then were treated ± NT3 (optimal 2 nM, or suboptimal 0.2 nM) or PTPs (optimal: 40 nM, suboptimal 8 nM) ± the indicated agents (10 µM) for 20 min. Detergent lysates were analyzed by western blotting with anti-pTyr mAb 4G10, anti-phospho-pErk1,2 or anti-phospho-Akt (Cell Signaling). After stripping, membranes were re-probed with anti-actin (Sigma) or total anti-Erk1.2 or total anti-Akt (Cell Signaling) to standardize loading.

In silico modeling of TrkC bound to NT3 and PTPs, and docking of CP14

We used AlphaFold3 server (25) to model structures of the TrkC.T1 monomer (Uniprot Q16288-2) unliganded or bound to NT3 (Uniprot P20783) and PTPs ligands (PTPs is labeled here as

PTPRS). Because TrkC is activated as homodimer, and NT3 is a symmetrical homodimer, we modeled the complex with a 2:2:2 stoichiometry. Five models were calculated for each structure. The result gave good prediction scores for the interaction (ipTM > 0.5) and low position error among the subdomains (≤5 Å). Furthermore, the five models converged, with root mean square deviations between 0.8 and 1.2 Å for the extracellular domain of monomeric TrkC.T1 (a.a. 30–400), and 2.0–3.9 Å for the TrkC.T1–NT3–PTPRS dimer (again using only the extracellular portion of TrkC.T1). The binding of NT3 to the D5 subdomain (also known as IgG-C2), and PTPRS bound to the D1–D2 subdomain (also known as LRR), agree with previous published reports (12, 55).

For docking, we used the SeamDock server and the AutoDock Vina protocols (56) to create unbiased docking to the different receptor structures. Using this computational docking tool, we sought to determine the binding site for Cyclic-14-KI on both the TrkC-T1 monomer and the dimeric TrkC.T1–NT3–PTPRS complex. Initially, we used a large docking box to generate an unbiased hierarchy of docking sites, and then we used a smaller box on the top site centered on the D4–D5 subdomains. Ten binding modes were calculated for each run. The top three models had binding energies between –6.2 and –6.8 kcal/mol for the monomeric TrkC structure, and –6.4 to –6.7 kcal/mol for the dimeric TrkC.T1–NT3–PTPRS complex.

RP animal model

All animal procedures respected the IACUC guidelines for use of animals in research, and protocols approved by McGill University Animal Welfare Committees. All animals were housed 12 h dark–light cycle with food and water ad libitum. We used the "RHOP347S" transgenic mouse (expressing the human rhodopsin mutated at amino acid position 347) in a C57BL/6J (B6) background (28). This model of RP faithfully replicates features of disease progression in humans. Both male and female animals were used in the experiments, with no sex selection of the litters. Similar findings are reported for both sexes. Gender issues do not apply.

Retinal organotypic cultures

For retinal cultures, mice at PN 18 (weighing between 10 and 12 g) were used. Whole explants of retinas were used for organotypic culture experiments. Procedures were as described previously (15, 45, 57). Whole eyes were enucleated, and whole retinas dissected from WT and RHOP347S mice at PN 18 and immediately transferred into 24-well plates containing 500 μL of culture medium (DMEM/F12 supplemented with 10 mM NaHCO$_3$, 100 μg/mL transferrin, 100 μM putrescine, 20 nM progesterone, 30 nM Na$_2$SeO$_3$, 0.05 mg/mL gentamicin, 2 mM L-glutamine, and 1 mM sodium pyruvate). Then, the media were removed and replaced with fresh media containing the treatments or controls and incubated at 37 °C and 5% CO$_2$ for 24 h. Agent **16** or **CP14** was tested at a concentration of 10 μM, NT3 control at 20 nM. Cell-grade DMSO was used for vehicle control and was 0.5% by volume. Retinas were processed for TUNEL staining to evaluate photoreceptor cell death. Retinal flat mounts prepared form WT mice were used as negative controls, as they do not exhibit photoreceptor death in the time frame of the assay.

Quantification of TNF-α protein

RHOP347S retinas were cultured as organotypic explants and treated for 24 h with antagonists **16**, or **CP14**, or vehicle control. Lysates of whole retinas were quantified for TNF-α protein by western blots with anti-TNF-α mAb (PeproTech), standardized to protein loading by western blots using anti-actin mAb (Sigma).

TUNEL staining

Staining was performed as described (45, 57) using the DeadEnd Fluorometric TUNEL system (Promega). RHOP347S retinas in culture (n = 3) were first fixed in 4% PFA in PBS and kept at 4 °C overnight. Three quick washes in PBS-0.2% BSA were done the next day, followed by three 30-min permeabilization steps, using 2% Triton X-100 in PBS. Retinas were then incubated with 20 μg/mL proteinase K in PBS for 15 min, briefly refixed in 4% PFA in PBS for 30 min and washed again with PBS-0.2% BSA before being transferred into Eppendorf tubes. Samples were incubated with 50 μL of equilibration buffer for 20 min and then 25 μL of terminal deoxynucleotidyl transferase reaction mixture for 2.5 h at 37 °C. The reaction was terminated using a 30-min incubation of 2× saline sodium citrate solution. The retinas were mounted with the ganglion cell layer facing up, using Vectashield with 4′,6-diamidino-2-phenylindole.

Fluorescence microscopy, image acquisition, and data analysis

Pictures were taken as Z-stacks of confocal optical sections using a Leica confocal microscope at a 20× objective. Images were equally adjusted using Adobe Photoshop CS 8.0 to remove background signals. The retinas were divided into four quadrants and three concentric areas as depicted in Fig. 6C. For quantification, image acquisition accounted for the different topological density of photoreceptors (higher numbers in the central region and lower numbers in the periphery). In the photoreceptor layer one picture was taken for each of the three areas (central, middle and periphery) in each quadrant for a total of 12 images per each retina, at 20×. Total TUNEL$^+$ cells were counted semi-automatically (ImageJ) (45, 57). Analyses compared the drug-treated explants vs. vehicle-treated cultures, in explants from WT control mice and from RHOP347S transgenic mice.

In vivo therapy in RHOP347S mice

Intravitreal injections were performed in RHOP347S mice, at PN18, with ongoing disease and significant preexisting photoreceptor loss. Injection procedures are as previously described (44). Briefly, a total volume of 1 μL of vehicle (PBS) or compound **16** (1 mM) or **CP14** (1 mM) was slowly delivered into the RHOP347S mouse vitreous chamber using a Hamilton syringe under a stereotactic microscope. After the injection, the syringe was left in place for 30 s and slowly withdrawn to prevent efflux. Given the severity of the disease model, with rapid degeneration, only 1× drug delivery was done at PN18 and retinas were evaluated at PN20.

Analyses of photoreceptors after in vivo therapy in RHOP347S mice

At PN20 (on day 2 after intravitreal injection), the eyes were enucleated, and serial retinal sections were prepared with distances from the ON recorded to account for quadrants and location (Fig. 6C). The presence of dead photoreceptors was evaluated in TUNEL assays described above. In the same tissues from the vehicle or CP14-treated animals, the presence of surviving photoreceptors was quantified using hematoxylin and eosin staining (H&E, catalog H-3502; Vector) of retinal sections (12 μm). The stain reveals the nucleus and cytoplasm of the live photoreceptors in the photoreceptor layer, morphologically distinct from Müller cells and retinal ganglion cells which in any case are in a different

anatomical layer. Bright field Imaging of the stained RHOP347S retinas under 40× magnification was done using a Zeiss apotome three microscope. Sections were prepared as defined for the central (area 1), middle (area 2), and peripheral (area 3) regions (respectively 100–1,000 μm, 1,000–2,000 μm, and >2,000 μm from the center of the optic nerve head). The number of photoreceptor nuclei on retinal sections was evaluated by manually counting H&E-stained nuclei in the ONL. The counts were averaged from 8 to 12 regions of interest from 3 to 4 sections of the same retina, and the mean were calculated for each group.

Statistical analyses

The quantitative data were subjected to statistical analyses using GraphPad Prism 5 software and are presented as mean ± SD of the indicated independent experiments. One-way ANOVA was used for all comparisons between groups with significance $\alpha < 0.05$ followed by Bonferroni's correction for multicomparisons. For ex vivo and in vivo studies, data were subjected to statistical analyses using GraphPad Prism 5 software and are presented as mean ± SD for a whole retina or per each area of the retina to account for the natural thinning of the photoreceptor layer (thicker in center and thinner in periphery). One-way ANOVA was used for all comparisons between groups with significance $\alpha < 0.05$ followed by Bonferroni's correction for multicomparisons.

Supplementary Material

Supplementary material is available at *PNAS Nexus* online.

Author Contributions

F.B., H.N., A.G., and C.O. designed, planned, and carried out experiments, curated, analyzed, and cross-validated their data, and prepared most figures and tables after conducting statistical analysis. R.G. statistically analyzed and prepared a figure. F.B. and H.U.S. produced the monoclonal antibodies. H.N. carried out the synthesis and characterization of the small molecules. J.-F.T. carried out the computational modeling, docking, and corresponding figures. H.U.S. generated the concept, helped design experiments, supervised the work, and lead the organization and writing of the manuscript. The iterative editing of versions of the manuscript had contributions primarily from F.B. and H.N. All authors reviewed and approved the final version of the manuscript. Authors agreed to the order in which they are listed. All authors contributed to the article and approved the submitted version.

Data Availability

The data that support the findings of this study are openly available in Figshare.com at https://figshare.com/articles/dataset/ My_Data/28024736/1 reference number. The research materials published in this study may be available by signing an institutional Material Transfer Agreement, that can be requested from the corresponding author, H.U.S. at uri.saragovi@mcgill.ca.

References

1 Rudzinski M, Wong TP, Saragovi HU. 2004. Changes in retinal expression of neurotrophins and neurotrophin receptors induced by ocular hypertension. *J Neurobiol*. 58:341–354.

2 Szobota S, *et al.* 2019. BDNF, NT-3 and Trk receptor agonist monoclonal antibodies promote neuron survival, neurite extension, and synapse restoration in rat cochlea ex vivo models relevant for hidden hearing loss. *PLoS One*. 14:e0224022.

3 Deinhardt K, Chao MV. 2014. Trk receptors. *Handb Exp Pharmacol*. 220:103–119.

4 Tessarollo L, *et al.* 1997. Targeted deletion of all isoforms of the trkC gene suggests the use of alternate receptors by its ligand neurotrophin-3 in neuronal development and implicates trkC in normal cardiogenesis. *Proc Natl Acad Sci U S A*. 94:14776–14781.

5 Youn YH, Feng J, Tessarollo L, Ito K, Sieber-Blum M. 2003. Neural crest stem cell and cardiac endothelium defects in the TrkC null mouse. *Mol Cell Neurosci*. 24:160–170.

6 Bai Y, *et al.* 2010. In glaucoma the upregulated truncated TrkC.T1 receptor isoform in glia causes increased TNF-alpha production, leading to retinal ganglion cell death. *Invest Ophthalmol Vis Sci*. 51:6639–6651.

7 Harada T, *et al.* 2000. Modification of glial-neuronal cell interactions prevents photoreceptor apoptosis during light-induced retinal degeneration. *Neuron*. 26:533–541.

8 Palko ME, Coppola V, Tessarollo L. 1999. Evidence for a role of truncated trkC receptor isoforms in mouse development. *J Neurosci*. 19:775–782.

9 Esteban PF, *et al.* 2006. A kinase-deficient TrkC receptor isoform activates Arf6-Rac1 signaling through the scaffold protein tamalin. *J Cell Biol*. 173:291–299.

10 Brahimi F, *et al.* 2016. The paradoxical signals of two TrkC receptor isoforms supports a rationale for novel therapeutic strategies in ALS. *PLoS One*. 11:e0162307.

11 Brahimi F, *et al.* 2020. Alternative splicing of a receptor intracellular domain yields different ectodomain conformations, enabling isoform-selective functional ligands. *iScience*. 23:101447.

12 Coles CH, *et al.* 2014. Structural basis for extracellular cis and trans RPTPsigma signal competition in synaptogenesis. *Nat Commun*. 5:5209.

13 Takahashi H, *et al.* 2011. Postsynaptic TrkC and presynaptic PTPsigma function as a bidirectional excitatory synaptic organizing complex. *Neuron*. 69:287–303.

14 Saragovi HU, Galan A, Levin LA. 2019. Neuroprotection: prosurvival and anti-neurotoxic mechanisms as therapeutic strategies in neurodegeneration. *Front Cell Neurosci*. 13:231.

15 Galan A, *et al.* 2017. In retinitis pigmentosa TrkC.T1-dependent vectorial Erk activity upregulates glial TNF-alpha, causing selective neuronal death. *Cell Death Dis*. 8:3222.

16 Galan A, *et al.* 2014. Neuronal injury external to the retina rapidly activates retinal glia, followed by elevation of markers for cell cycle re-entry and death in retinal ganglion cells. *PLoS One*. 9:e101349.

17 Brahimi F, Ko E, Malakhov A, Burgess K, Saragovi HU. 2014. Combinatorial assembly of small molecules into bivalent antagonists of TrkC or TrkA receptors. *PLoS One*. 9:e89617.

18 LeSauteur L, Wei L, Gibbs BF, Saragovi HU. 1995. Small peptide mimics of nerve growth factor bind TrkA receptors and affect biological responses. *J Biol Chem*. 270:6564–6569.

19 LeSauteur L, Cheung NK, Lisbona R, Saragovi HU. 1996. Small molecule nerve growth factor analogs image receptors in vivo. *Nat Biotechnol*. 14:1120–1123.

20 Zaccaro MC, *et al.* 2005. Selective small molecule peptidomimetic ligands of TrkC and TrkA receptors afford discrete or complete neurotrophic activities. *Chem Biol*. 12:1015–1028.

21 Brahimi F, *et al.* 2009. A peptidomimetic of NT-3 acts as a TrkC antagonist. *Peptides*. 30:1833–1839.

22 Chen D, *et al.* 2009. Bivalent peptidomimetic ligands of TrkC are biased agonists and selectively induce neuritogenesis or potentiate neurotrophin-3 trophic signals. *ACS Chem Biol*. 4:769–781.

23 Liu J, Brahimi F, Saragovi HU, Burgess K. 2010. Bivalent diketopiperazine-based tropomysin receptor kinase C (TrkC) antagonists. *J Med Chem*. 53:5044–5048.

24 Ultsch MH, *et al.* 1999. Crystal structures of the neurotrophin-binding domain of TrkA, TrkB and TrkC. *J Mol Biol*. 290:149–159.

25 Abramson J, *et al.* 2024. Accurate structure prediction of biomolecular interactions with AlphaFold 3. *Nature*. 630:493–500.

26 Robinson RC, *et al.* 1999. The structures of the neurotrophin 4 homodimer and the brain-derived neurotrophic factor/neurotrophin 4 heterodimer reveal a common Trk-binding site. *Protein Sci*. 8:2589–2597.

27 Robinson RC, Radziejewski C, Stuart DI, Jones EY. 1995. Structure of the brain-derived neurotrophic factor/neurotrophin 3 heterodimer. *Biochemistry*. 34:4139–4146.

28 Li T, Snyder WK, Olsson JE, Dryja TP. 1996. Transgenic mice carrying the dominant rhodopsin mutation P347S: evidence for defective vectorial transport of rhodopsin to the outer segments. *Proc Natl Acad Sci U S A*. 93:14176–14181.

29 Hartong DT, Berson EL, Dryja TP. 2006. Retinitis pigmentosa. *Lancet*. 368:1795–1809.

30 Bai Y, *et al.* 2010. In glaucoma the up-regulated truncated TrkC.T1 receptor isoform in glia causes increased TNF-alpha production, leading to retinal ganglion cell death. *Invest Ophthalmol Vis Sci*. 51:6639–6651.

31 Brahimi F, *et al.* 2010. A monovalent agonist of TrkA tyrosine kinase receptors can be converted into a bivalent antagonist. *Biochim Biophys Acta*. 1800:1018–1026.

32 Takeda A, Yanai R, Murakami Y, Arima M, Sonoda KH. 2020. New insights into immunological therapy for retinal disorders. *Front Immunol*. 11:1431.

33 Lee SJ, *et al.* 2023. Metabolic transcriptomics dictate responses of cone photoreceptors to retinitis pigmentosa. *Cell Rep*. 42:113054.

34 Olivares-Gonzalez L, Velasco S, Millan JM, Rodrigo R. 2020. Intravitreal administration of adalimumab delays retinal degeneration in rd10 mice. *FASEB J*. 34:13839–13861.

35 Cueva Vargas JL, *et al.* 2015. Soluble tumor necrosis factor alpha promotes retinal ganglion cell death in glaucoma via calcium-permeable AMPA receptor activation. *J Neurosci*. 35:12088–12102.

36 Nakazawa T, *et al.* 2006. Tumor necrosis factor-alpha mediates oligodendrocyte death and delayed retinal ganglion cell loss in a mouse model of glaucoma. *J Neurosci*. 26:12633–12641.

37 Bitsche M, *et al.* 2011. Neurotrophic receptors as potential therapy targets in postnatal development, in adult, and in hearing loss-affected inner ear. *Otol Neurotol*. 32:761–773.

38 Kempfle JS, *et al.* 2021. A novel small molecule neurotrophin-3 analogue promotes inner ear neurite outgrowth and synaptogenesis in vitro. *Front Cell Neurosci*. 15:666706.

39 Takahashi M, Sanchez JT. 2020. Effects of neurotrophin-3 on intrinsic neuronal properties at a central auditory structure. *Neurosci Insights*. 15:2633105520980442.

40 Blasco-Gutierrez MJ, Jose-Crespo IJ, Zozaya-Alvarez E, Ramos-Sanchez R, Garcia-Atares N. 2007. Trkc: a new predictive marker in breast cancer? *Cancer Invest*. 25:405–410.

41 Jin W, *et al.* 2010. Trkc plays an essential role in breast tumor growth and metastasis. *Carcinogenesis*. 31:1939–1947.

42 Bai Y, *et al.* 2010. Chronic and acute models of retinal neurodegeneration TrkA activity are neuroprotective whereas p75NTR activity is neurotoxic through a paracrine mechanism. *J Biol Chem*. 285:39392–39400.

43 Galan A, *et al.* 2017. Subconjunctival delivery of p75NTR antagonists reduces the inflammatory, vascular, and neurodegenerative pathologies of diabetic retinopathy. *Invest Ophthalmol Vis Sci*. 58:2852–2862.

44 Barcelona PF, *et al.* 2016. p75NTR and its ligand ProNGF activate paracrine mechanisms etiological to the vascular, inflammatory, and neurodegenerative pathologies of diabetic retinopathy. *J Neurosci*. 36:8826–8841.

45 Jmaeff S, *et al.* 2020. Small-molecule ligands that bind the RET receptor activate neuroprotective signals independent of but modulated by coreceptor GFRalpha1. *Mol Pharmacol*. 98:1–12.

46 Platon-Corchado M, *et al.* 2017. P75(NTR) antagonists attenuate photoreceptor cell loss in murine models of retinitis pigmentosa. *Cell Death Dis*. 8:e2922.

47 Bruno MA, *et al.* 2004. Long-lasting rescue of age-associated deficits in cognition and the CNS cholinergic phenotype by a partial agonist peptidomimetic ligand of TrkA. *J Neurosci*. 24:8009–8018.

48 Xhima K, *et al.* 2022. Ultrasound delivery of a TrkA agonist confers neuroprotection to Alzheimer-associated pathologies. *Brain*. 145:2806–2822.

49 Xhima K, *et al.* 2020. Focused ultrasound delivery of a selective TrkA agonist rescues cholinergic function in a mouse model of Alzheimer's disease. *Sci Adv*. 6:eaax6646.

50 Josephy-Hernandez S, *et al.* 2019. Pharmacological interrogation of TrkA-mediated mechanisms in hippocampal-dependent memory consolidation. *PLoS One*. 14:e0218036.

51 Sarthy VP, *et al.* 1998. Establishment and characterization of a retinal Muller cell line. *Invest Ophthalmol Vis Sci*. 39:212–216.

52 Guillemard V, *et al.* 2010. An agonist mAb directed to the TrkC receptor juxtamembrane region defines a trophic hot spot and interactions with p75 coreceptors. *Dev Neurobiol*. 70:150–164.

53 Baell JB, Holloway GA. 2010. New substructure filters for removal of pan assay interference compounds (PAINS) from screening libraries and for their exclusion in bioassays. *J Med Chem*. 53:2719–2740.

54 Maliartchouk S, Saragovi HU. 1997. Optimal nerve growth factor trophic signals mediated by synergy of TrkA and p75 receptor-specific ligands. *J Neurosci*. 17:6031–6037.

55 Murail S, de Vries SJ, Rey J, Moroy G, Tuffery P. 2021. SeamDock: an interactive and collaborative online docking resource to assist small compound molecular docking. *Front Mol Biosci*. 8:716466.

56 Trott O, Olson AJ. 2010. AutoDock Vina: improving the speed and accuracy of docking with a new scoring function, efficient optimization, and multithreading. *J Comput Chem*. 31:455–461.

57 Jmaeff S, Sidorova Y, Nedev H, Saarma M, Saragovi HU. 2020. Small-molecule agonists of the RET receptor tyrosine kinase activate biased trophic signals that are influenced by the presence of GFRa1 co-receptors. *J Biol Chem*. 295:6532–6542.